Electrochemical Impedance Spectroscopy (EIS) Characterization of Reformate-operated High Temperature PEM Fuel Cell Stack

Sahlin, Simon Lennart; Simon Araya, Samuel; Andreasen, Søren Juhl; Kær, Søren Knudsen

Published in:
International Journal of Power and Energy Research

DOI (link to publication from Publisher):
10.22606/ijper.2017.11003

Publication date:
2017

Document Version
Publisher's PDF, also known as Version of record

International Journal of Power and Energy Research, Vol. 1, No. 1, April 2017
https://dx.doi.org/10.22606/ijper.2017.11003

Electrochemical Impedance Spectroscopy (EIS) Characterization of Reformate-operated High Temperature PEM Fuel Cell Stack

Simon Lennart Sahlin, Samuel Simon Araya, Søren Juhl Andreasen and Søren Knudsen Kær

Department of Energy Technology, Aalborg Universitet, AAU,
Pontoppidanstræde 111, 9220 Aalborg Øst, Denmark
Email: sls@et.aau.dk

Abstract This paper presents an experimental characterization of a high temperature proton exchange membrane fuel cell (HT-PEMFC) short stack carried out by means of impedance spectroscopy. Selected operating parameters; temperature, stoichiometry and reactant compositions were varied to investigate their effects on a reformate-operated stack. Polarization curves were also recorded to complement the impedance analysis of the researched phenomena. An equivalent circuit model was used to estimate the different resistances at varying parameters. It showed a significantly higher low frequency resistance at lower stoichiometry. Both anode and cathode stoichiometric ratio had significant effects on the stack performance during the dry hydrogen and reformate operation modes. In both cases the effects faded away when sufficient mass transport was achieved, which took place at $\lambda_{anode} = 1.3$ for dry hydrogen, $\lambda_{anode} = 1.6$ for reformate operation and $\lambda_{cathode} = 4$. The work also compared dry hydrogen, steam reforming and autothermal reforming gas feeds at 160 °C and showed appreciably lower performance in the case of autothermal reforming at the same stoichiometry, mainly attributable to mass transport related issues. In a CO poisoning analysis the stack showed good tolerance to concentration up to 1% CO in the fuel stream.

Keywords: HTPEM, electrochemical impedance spectroscopy, fuel cell, degradation.

1 Introduction

Technology readiness for fuel cells is as much about ensuring that they deliver the required power output for the intended application as it is about proving that they are as cost-effective and as durable as competing technologies. High temperature PEM fuel cells (HT-PEMFC) are intended to replace diesel generator sets for back up applications, heat and gas engines and boilers for micro combined heat and power (Micro-CHP) applications among other devices. In order to compete with these mature technologies and take advantage of their renewable edge over traditional devices, they have to be improved in performance, durability and their cost has to be reduced significantly.

In recent years, HT-PEMFCs operated above 100 °C have been researched extensively due to the advantages they offer compared to low temperature PEM fuel cells (LT-PEMFC). Their increased operating temperature allows for increased electrode kinetics, easier heat and water management, the possibility of useful waste heat recovery to increase overall efficiency and increased tolerance to fuel impurities such as Carbon Monooxide (CO) [6, 7, 33, 43]. These advantages in turn lead to simpler design and the use of reformate mixtures of various fuel sources with little or no pre-purification translates into lower costs[7, 24, 43].

Despite the significant advances in the technology and the presence of several commercial products, there are still opportunities for further understanding and enhancements in terms of degradation and durability. Degradation due to CO is mainly associated with reduced free reaction sites due to its adsorption on the Pt electrode surface [6, 17, 21]. It is an effect that can be reversed after reconditioning of the stack [44]. However, prolonged exposure to CO may cause irreversible degradation [11]. The poisoning effect of CO in HT-PEMFCs is reduced due to their higher operating temperature, where lower surface adsorption of CO on the Pt-surface combined with increased electro-oxidation of CO to CO_2 leads to a significant improvement in tolerance compared to LT-PEMFCs [3, 11, 15].

Temperature is a crucial parameter for HT-PEMFCs, as it is the parameter that gives them the edge over their lower temperature counter parts in terms of improved tolerance to impurities, easier water managements and simpler system design. However, its increase also enhances stack degradation and material challenges, by increasing mechanical and thermal stresses [33, 45].

Like temperature, stiochiometry also depends on conflicting considerations; optimization of fuel utilization without causing significant mass transport losses. Galbiati et al. [13] showed that stoichiometry also affects water transport, where increasing air stoichiometry reduces water transport from cathode, because it enhances water removal on that side, resulting in lower anode exhaust water flow and higher hydrogen stoichiometry increases water transport from cathode leading to higher water flux in the anode exhaust.

These effects like other parametric characterizations have been extensively studied both by model simulations and single cell testing for fundamental understanding of degradation mechanisms [3, 12, 19, 36, 37]. This work extends the study of parametric characterization to stack level in order to understand the fundamentals at a step closer to real life applications. It investigates the effects of temperature, stoichiometry and CO poisoning in an HT-PEMFC short stack. Characterization was done by means of electrochemical impedance spectroscopy (EIS) and polarization curves under varying operating conditions.

Impedance spectroscopy is a strong electrochemical characterization tool that can be used in-situ to obtain several valuable information about a device's electrochemical operation. However, its interpretation by means of EC model fitting, though quick, can be highly ambiguous. Several equivalent circuit (EC) models can fit the same impedance data, and therefore, when choosing an EC model one should have a good knowledge of the behaviour of the tested device. Also, how the different phenomena in the fuel cells and its components contribute to the impedance spectra are not entirely clear.

In the case of HT-PEMFCs several EC models based on different combinations and modifications of Randles' circuit (electrolyte resistance in series with the parallel combination of the double-layer capacitance and a charge transfer resistance) have been proposed [5, 18, 34, 39]. Below is a brief literature review of the interpretation of impedance spectra and the corresponding EC model elements.

Impedance measurements of real fuel cell systems have a positive high frequency intercept and up to three arcs, depending on the extent of the mass transport effects. It is widely agreed that the high frequency intercept represents the sum of ohmic resistances of the cell components such as, the membrane, catalyst layer, gas diffusion layer, flow plates, and contact resistances of component connections [13, 41, 45].

Even though, it is difficult to discriminate among the different contributions to the ohmic resistance, its changes during fuel cell operation can be attributed to the changes in proton conductivity [18, 45]. Proton conduction takes place both in the membrane electrolyte and the electrolyte in the catalyst layer by means of proton hopping mechanism along anion chains formed from self-ionization and self-dehydration of H_3PO_4 [9, 45]. Kondratenko et al. [18] distinguish between the contributions of the membrane resistance and electrolyte resistances between catalyst sites in the active layer using an EC model with a transmission line. However, in the current work a simpler EC model is used and changes in ohmic resistance are attributed to the overall variations in conductivity.

The EC model fit of the impedance arc at high frequency gives high frequency resistance (R_{HF}).

Romero-Castañón et al. [30] associate this exclusively to the structural features of the membrane electrode assembly (MEA). Yuan et al. [41] argue that the impedance of the full fuel cell almost equals the cathode impedance due to the fast hydrogen oxidation reaction in H_2/O_2(air) operation [18]. Other authors distinguish between anode and cathode faradaic resistances, with the high frequency arc being the anode resistance and the intermediate frequency arc cathode resistance [5, 25]. According to Mench et al. [25] changes in low and intermediate frequency resistance provide insight into degradation mechanisms in the cathode catalyst layer, with the intermediate frequency time constant attributable to the charge transfers and lower frequency ones to mass transport. To avoid these ambiguities, in this work the analyses of the fitted resistances are not discriminated between anode and cathode, but rather into frequency ranges as high frequency resistance (R_{HF}), intermediate frequency resistances (R_{IF}) and low frequency resistance (R_{LF}).

To the knowledge of the authors there is no standardized way of representing impedance spectra and fitted data to date. In literature different representations of fuel cell impedance can be found, including, no units, Ohms (Ω) and Ωcm^2 (impedance normalized with respect to unit cell area) [14, 20, 29, 30]. Multiplying impedance and fitted EC model data with the active single cell area makes it easier to

compare EIS measurements of different single cell sizes. However, this does not allow comparability of impedance measurements of fuel cell stacks composed of different cell numbers, or comparability of single cell EIS to that of a fuel cell stack. In this work to allow for better comparability, EIS and EC fitted data are multiplied by the active cell area and divided by the number of cells in the fuel cell stack and represented with the unit Ωcm^2/cell.

2 Experimental Work

A schematic of the experimental setup is shown in Fig.1. A 15 cell, liquid-cooled (thermo-oil) high temperature PEM fuel cell stack from Serenergy A/S was investigated for its sensitivity to changes in operating parameters; temperature, stoichiometry and fuel composition. The cells are based on BASF Celtec P H_3PO_4-doped PBI membrane with active cell area of 163.5 cm^2. A picture of the tested stack is shown in Fig. 2.

Tests were carried out on a Greenlight Innovation fuel cell test stand, with a Reference 3000 from Gamry instruments for electrochemical impedance spectroscopy recording.

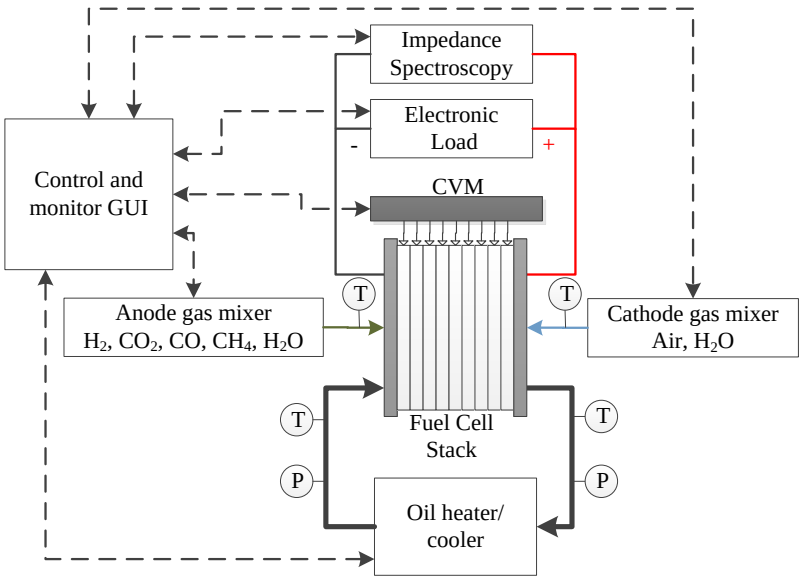

Figure 1. Test setup schematic

2.1 Test Procedures

To investigate the fuel cell stack's response to different parametric changes and different fuel compositions, the test matrix in Tab. 1 was used. First, the fuel cell break-in was done at 160 °C at a current density of 0.2 A/cm^2 for 18 hours, then temperature and stoichiometry were varied for three different fuel composition modes. The operation modes were chosen to simulate dry hydrogen operation, steam reforming (SR) and auto-thermal reforming(ATR) gas feeds. SR was simulated with 60% H_2, 15% H_2O, 24% CO_2 and CO levels from 0 to 1%, using nitrogen as make-up-gas, and ATR with 41% H_2, 8.5% H_2O, 50% CO_2 and 1% CO. The stoichiometry is based on the ratio between the required gas nessesary for the reaction and the available gas at the inlet.

ATR is included here because it is commonly used in commercial methane-based fuel cell systems. The process can be advantageous as it brings about fast system start-up time and simplified system design since the system can be operated without external heat supply. Systems using ATR are often supplied

Table 1. Test matrix. N_2 is used for make-up gas

Anode:Pure-dry hydrogen				
Index	**T (^{o}C)**	**Air stoic.**	**H_2 Stoic.**	**CO (%)**
1	**150**	3.5	1.35	
2	**155**	3.5	1.35	
3	**160**	3.5	1.35	
4	**165**	3.5	1.35	
5	**170**	3.5	1.35	
6	**175**	3.5	1.35	
7	160	**2**	1.35	
8	160	**2.5**	1.35	
9	160	**3**	1.35	
10	160	**3.5**	1.35	
11	160	**4**	1.35	
12	160	3.5	**1.25**	
13	160	3.5	**1.3**	
14	160	3.5	**1.35**	
15	160	3.5	**1.4**	
Anode: Methane reformate gas simulation (60% H_2, 15% H_2O)				
Index	**T (^{o}C)**	**Air stoic.**	**H_2 Stoic.**	**CO (%)**
16	**155**	3.5	1.35	0.8
17	**160**	3.5	1.35	0.8
18	**165**	3.5	1.35	0.8
19	**170**	3.5	1.35	0.8
20	**175**	3.5	1.35	0.8
21	160	3.5	1.35	**0.25**
22	160	3.5	1.35	**0.5**
23	160	3.5	1.35	**1**
24	160	3.5	**1.6**	0.8
25	160	3.5	**1.3**	0.8
26	160	3.5	**1.35**	0.8
27	160	3.5	**1.5**	0.8
28	160	**2**	1.35	0.8
29	160	**2.5**	1.35	0.8
30	160	**3**	1.35	0.8
31	160	**3.5**	1.35	0.8
Anode: ATR gas simulation (41%H_2, 8.5% H_2O)				
Index	**T (^{o}C)**	**Air stoic.**	**H_2 Stoic.**	**CO (%)**
32	**160**	3.5	1.35	1
33	**165**	3.5	1.35	1
34	**170**	3.5 -	1.35	1
35	**175**	3.5	1.35	1

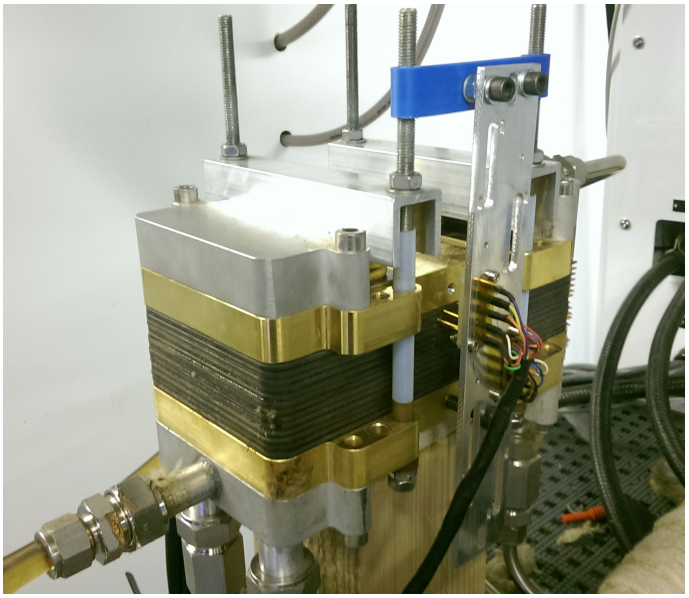

Figure 2. A picture of the tested short stack

with an additional water-gas-shift gas cleaning unit[4]. The introduction of oxygen in ATR process was studied by Salemme et al. [31], where both ATR and SR reactions were investigated with regards to efficiency. They found that the efficiency of SR reaction is significantly higher compared to ATR reaction. The highest efficiency was found with methane (gas) steam reforming at 50.3% and methanol (liquid) at 46.9%. The maximum energy efficiency is defined according to (1)

$$\eta = \frac{P_e}{(n_f + n_{f,B}) \cdot \mathrm{LHV}} \tag{1}$$

where P_e is the electric power generated by the fuel cell, n_f is the inlet molar flow rate to the reforming reactor, $n_{f,B}$ is the molar flow rate to the burner, and LHV is the lower heating value of fuel.

Polarization curves and electrochemical impedance spectroscopy are the techniques of choice in this work and they were recorded at all stages of the experiments. Polarization curves were recorded until 1 A/cm^2 on dry hydrogen and until 0.6 A/cm^2 on reformate gas, as higher current densities resulted in poorer cell performances under reformate gas feed. The recording was stopped when the minimum cell voltage reached 0.2 V to prevent permanent damages to individual cells. The polarization curve is performed with a sweep from low to high at 2 A and a sweep from high to low at 4 A to avoid hysteresis phenomenons[42].

After each polarization an EIS spectrum was recorded between 10 kHz and 0.1 Hz. The measurements were carried out in galvanostatic mode at DC load of 33 A (0.2 $\frac{A}{cm^2}$) and an AC amplitude of 1.5 A current sinusoidal.

2.2 Equivalent Circuit Model Selection

The impedance measurements of the fuel cell stack used in these investigations show three distinct arcs as the impedance spectra in Fig. 4 illustrate. This implies three time constants that correspond to three characteristic frequency intervals are present. Hence, an EC model made up of three Resistance (R) - constant phase element (CPE) loops as shown in Fig.3 is used for impedance data interpretations, similarly to [35, 45]. An ideal resistance in series with the three arcs represents the real axis intercept of the impedance. In literature the high frequency vertical drag of the impedance below this intercept point is usually represented by an ideal inductor for wiring inductance contributions [5, 45]. However, in this work it can be seen that the wiring inductance is no longer a vertical line below the real axis but it bends towards the right. To account for this it is represented by an L-R arc in the EC model Fig. 3. This loop is

not used to characterize the stack, but simply to correct for the wiring artefacts and to make sure that the real axis intercept is correctly estimated for ohmic resistance evaluation.

The impedances of the circuit elements used in the model are given below as functions of frequency [40]:

$$Z_R(\omega) = R \tag{2}$$

$$Z_L(\omega) = i\omega L \tag{3}$$

$$Z_{CPE}(\omega) = Q^{-1}(i\omega)^{-n} \tag{4}$$

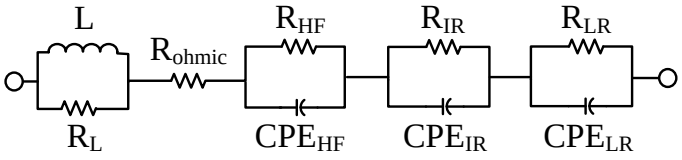

Figure 3. EC model representation of HT-PEMFC stack used in this work

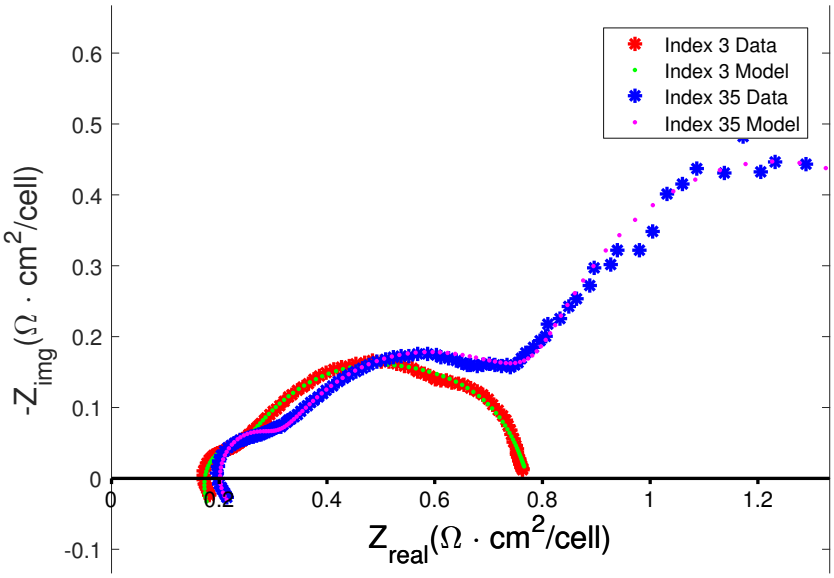

Figure 4. Examples of curve fitting using the EC model in Fig. 3
. Indices 3 and 35 represent the respective test points in Tab. 1

where, $Z_R(\omega)$ is the impdance of a Resistor $[\Omega]$, R is the resistance $[\Omega]$, $Z_L(\omega)$ is the impedance of an inductor $[\Omega]$, $Z_{CPE}(\omega)$ is the impedance of a CPE $[\Omega]$, and ω is the frequency [rad/s].

CPE is a pseudo-capacitor used in place of capacitors to fit EC models to real systems' impedance responses. It is used to depress the center of Nyquist plot semi-circle arcs to below the real axis as observed in real systems [40]. In eqn. 4, Q is the pseudo-capacitance $[\Omega^{-1}\mathrm{s}^{\mathrm{n}}\mathrm{cm}^{-2}]$ and n is the CPE exponent that characterizes the phase shift. This coefficient determines the nature of a CPE and it represents pure capacitor when n equals to 1 [40]. In this work, n values of 0.95, 0.7 and 1 (pure capacitor) were used for high, intermediate and low frequency arcs, respectively. These values are chosen based on the best fits and then kept constant to allow only the resistances to change during the fitting. The data in this work is fitted with a Matlab tool, called Z-fit [10].

3 Results and Discussion

3.1 Varying Temperature

The effects of temperature were tested for dry hydrogen operation and reformate conditions. It was varied at a step of 5 °C between 150 °C and 175 °C under dry hydrogen operation and between 160 °C and 175 °C under reformate operation mode. The minimum operating temperature was raised in the case of reformate condition to avoid degradation due to poisoning at lower temperature.

Dry hydrogen operation: The overall effect of temperature on the performance of a PBI based HT-PEMFC stack can be said negligible with slight tendency to increase with increasing temperature in the range between 150 °C and 175 °C as the polarization curves in Fig. 5 (a) show. This is consistent with the literature, where a slight increase in performance with increasing temperature is observed [23, 38]. The increase in performance is less marked in this work, because smaller temperature steps of 5 °C are used compared to 20 °C steps in the cited papers.

EIS measurements reveal more details that are not visible in the polarization curves. In Fig. 5 (b) it can be seen that impedance spectra move towards the right with increasing temperature, while also shrinking in the frequency range between 1 kHz and 10 Hz. The rightward movement of the real axis intercept of the impedance spectra is represented by changes in ohmic resistance (R_{ohmic}) in Fig. 6. It increases slightly with increasing temperature and can be attributed to the overall increase in contact resistances, including the membrane conductivity of the fuel cell stack. It appears as though the membrane conductivity decreases with increase in temperature, which is contrary to most literature[22, 38]. However, there are cases where the ohmic resistance decreases with increasing temperature until around 160 °C, and then increases for further increase in temperature [16, 36].

The reports in literature focus on ex-situ membrane conductivity or single cell impedance measurements, where the contact resistances are not significant. However, the membrane is not the only element contributing to the ohmic resistance. It is the sum of electrical contact resistances, where all the conductors and insulators present in the fuel cell stack between the current collectors are also contributors. The membrane can be considered as an electrical insulator and theoretically its resistance decreases with increasing temperature. In the current work it is seen that the total ohmic resistance increases with temperature and this may be caused by the increased electrical resistance of the conductive components, such as the flow plates and the current collectors, which in the case of a fuel cell stack are more significant compared to single cell measurements due to increased number of contact points.

The intermediate frequency was found to be constant constant between 150 °C and 175 °C, while the low frequency resistance seems to decrease slightly with increasing temperatures. R_{HF} shows a slight decrease from 155 °C to 160 °C with a small tendency to increase with temperature thereafter. This implies that charge transfer is not enhanced above 160 °C. In their unit cell tests, Su et al. [38] showed that increasing temperature enhances the cell performance due to the increase in reaction rate and mass transfer rate, which is partly confirmed in this work with slightly decreasing R_{LF}. Therefore, slight improvements in mass transport and high frequency charge transfer until 160 °C can be said to be the main cause of the slight performance enhancement achieved with increasing temperature.

Reformate conditions Even though HT-PEMFCs have the advantage of working efficiently under anhydrous conditions compared to LT-PEMFCs, humidification still improves the performance by increasing the proton conductivity of the polymer membrane [8]. Water also hydrates phosphoric acid (PA) and ensures a more uniform distribution of PA, thereby reducing PA poisoning effect which happens when PA and H_2 reduced polyphosphoric acid species block Pt surface area [28]. However, it is also reported that if water condenses inside the MEA it can cause PA leaching and thereby reduce the proton conductivity [22]. Therefore, it is important that water is removed in vapor phase before the fuel cell stack is cooled down for shutdown.

Figure 7 shows the effect of temperature under reformate gas operation mode.

Similarly to dry H_2 tests, the increase in temperature causes a slight increase in ohmic resistance. This increase in ohmic resistance could be related to the membrane swelling caused by water uptake [1, 22], or increase in the contact resistance due to the presence of several contact points at stack level.

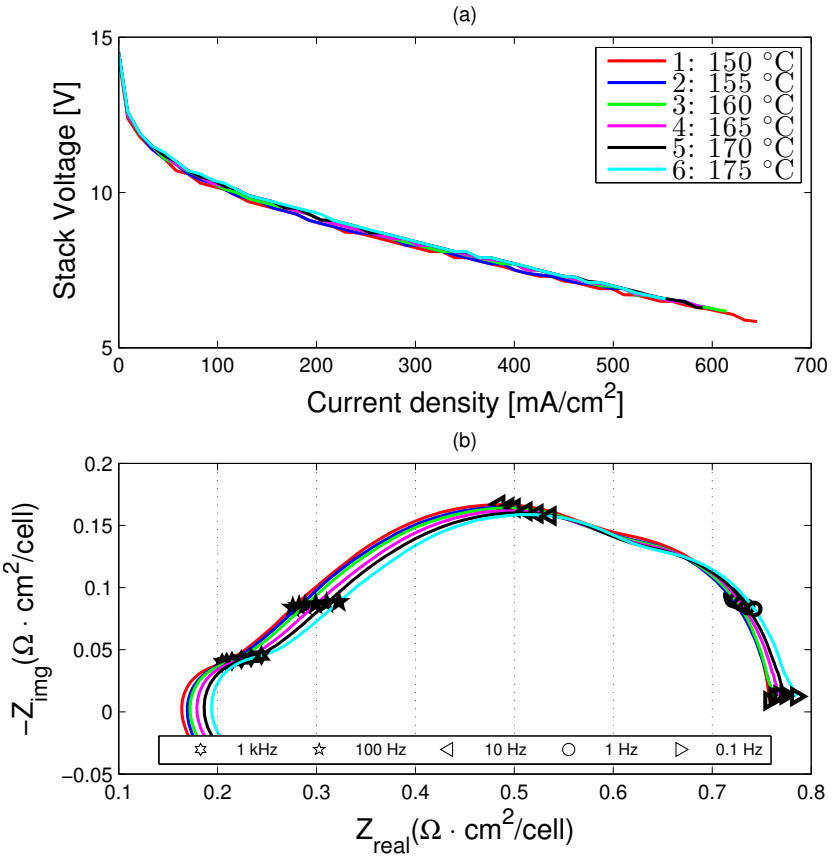

Figure 5. Effects of temperature under dry H_2 operation

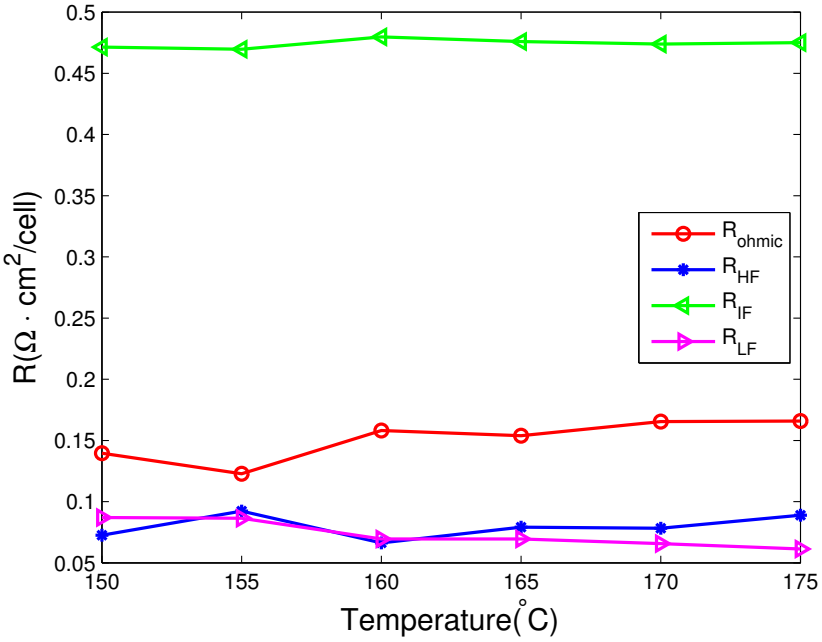

Figure 6. Effects of temperature under dry H_2 operation

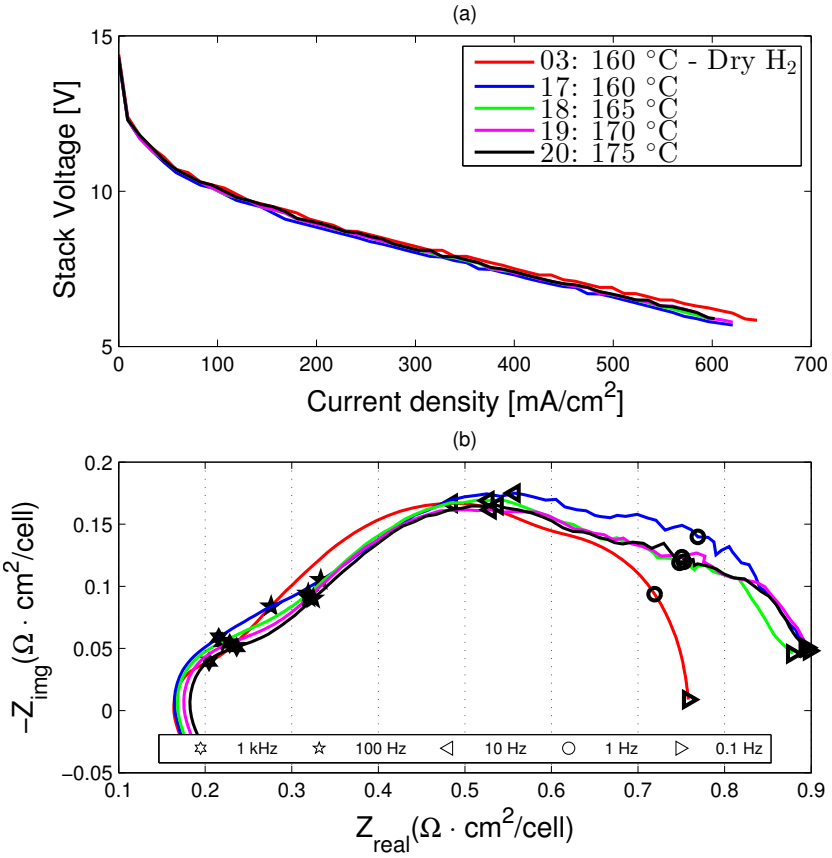

Figure 7. Temperature test under reformate gas operation

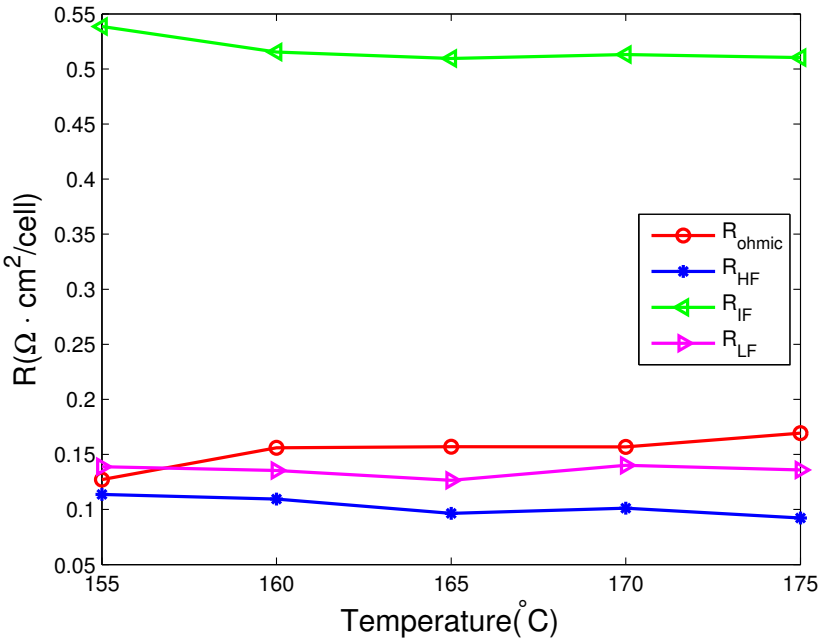

Figure 8. Effects of temperature under reformate gas operation

On the contrary, the polarization curves in Fig. 7(a) show a mild increase in performance with increasing temperature under reformate conditions, which are in-line with the expected effects of temperature.

Figure 8 shows the fitted resistances during wet reformate gas operation. Both R_{HF} and R_{IF} show a slight decrease with temperature in accordance with the overall increase in fuel cell stack performance in the corresponding polarization curves, Fig. 7(a). Unlike the case of dry hydrogen, a slight performance enhancement beyond 160 °C is seen under reformate conditions. This could be due to the presence of water which reduces the PA poisoning effect on Pt reaction sites by hydrating PA molecules [28].

3.2 Varying Stoichiometric Ratio

To improve fuel utilization without recirculation pumps different anode and cathode stoichiometric ratios were tested both under dry and reformate gas operation modes. Below are the EIS and polarization curve analyses of the fuel cell stack's response to different fuel compositions at different stoichiometric ratios.

Anode stoichiometry Figure 9 shows how hydrogen stoichiometry influences the performance on dry hydrogen feed. The fuel cell stack is tested from $\lambda_{anode} = 1.25$ to 1.4. The polarization curves show a decrease in performance at lower stoichiometries and the frequency response shows significant changes in resistance at lower frequencies which corresponds well with mass transport issues.

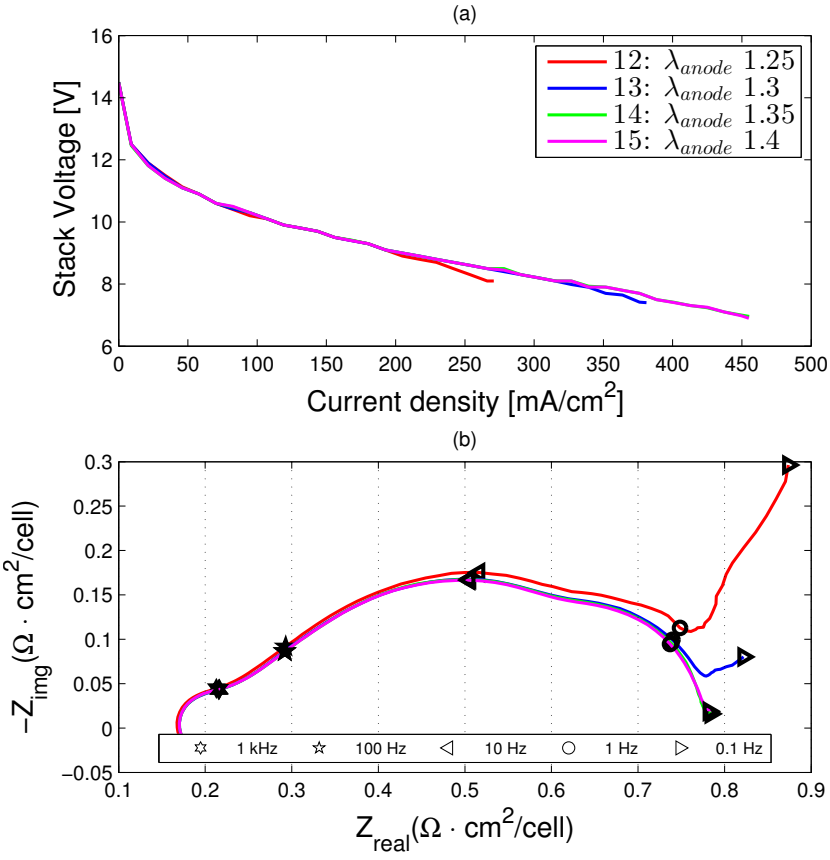

Figure 9. Impedance plot with different hydrogen stoichiometry levels with dry H_2

In Fig. 10, the fitted results show significant decrease in low frequency resistance. It can be seen that changes in stiochiometric ratio affect mainly the mass transport. It can also be seen that above $\lambda_{anode} = 1.3$ the decrease in R_{LF} is arrested, which indicates that once H_2 starvation is avoided increase in

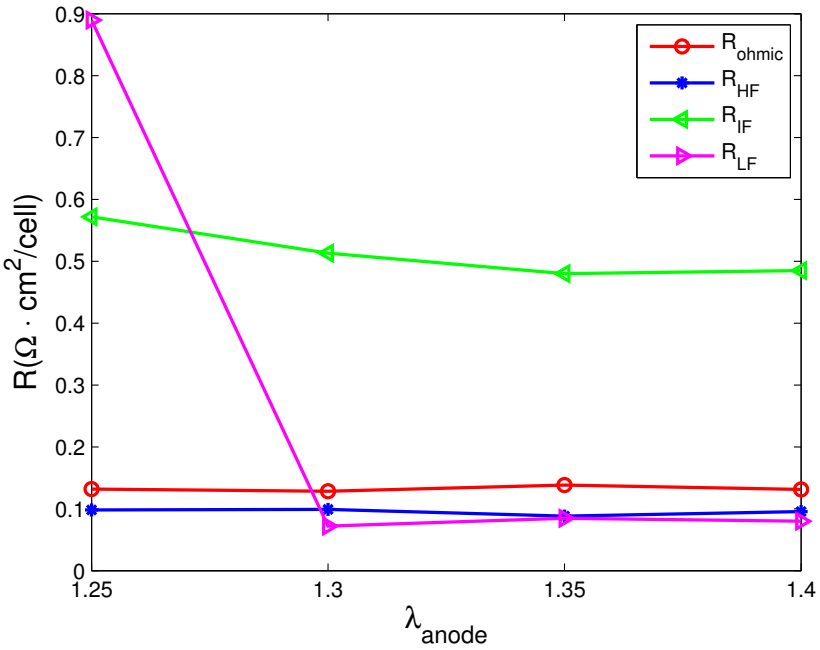

Figure 10. Impedance plot with different hydrogen stoichiometry levels with dry H_2

stiochiometry does not improve the fuel cell stack performance. It is also reported that both hydrogen and air stoichiometry affect water transport in a fuel cell with high λ_{anode} diminishing the anode water concentration [13]. However, these correlations and their impact on a stack performance are not clear and need further investigations.

In the case of reformate gas operation in Fig. 11(a) it can be seen that there is a larger spread in the polarization curves. λ_{anode} was changed between 1.3 to 1.6. Similarly to the dry hydrogen operation, the impedance plots show small changes between 10 Hz and 1 Hz and marked changes below 1 Hz. This implies that the effects are also in this case mainly attributable to enhanced mass transport with increasing λ_{anode}. Najafi et al. [26] found similar improvement under reformate gas conditions in the presence of CO when increasing anode stiochiometry from 1.2 to 1.6.

Both operation modes show a 45 ° line in the low frequency region below 1 Hz at low stoichiometry, Fig 9 and Fig. 11. Siegel et al. [34] noticed similar signature 45 ° line during fuel starvation. This is typical of mass transfer controlled frequency dependence, which is also sometimes called Warburg impedance [27, 40]. It is generated by diffusion problems at low frequency caused by hydrogen starvation at low stoichiometric ration. This can be avoided by working slightly above the critical lower stiochiometric ratio limit of 1.3 in the dry H_2 and 1.35 in reformate gas operation.

In this work mass transport is not modeled with Warburg diffusion but rather with a simple R-C loop to avoid more fitting uncertainties that can arise from introducing more variables of Warburg impedance. Also, not all the impedance spectra show a 45 ° diffusion line, hence, a model that can fit all the operating conditions has been used. It is worth mentioning that the appearance of such a signature 45 ° line on an impedance spectrum can be used to diagnose a fuel cell stack and to detect mass transport faults, and consequently intervene on the cause, which in this case is insufficient fuel from the reformer.

The fitted results shown in Fig. 12 also show a significant decrease in low frequency resistance with no significant changes in the intermediate and higher frequency ranges. R_{LF} decreases significantly from 1.3 to 1.35 and then slowly from 1.35 to 1.6.

These results can be used as a tool to evaluate a suitable stoichiometries both for dry hydrogen and reformate gas operation modes. While for dry hydrogen the performance improvement is arrested above λ_{anode} of 1.3, which is in line with the manufacture's specifications for dry hydrogen operation of 1.35 [32]. For reformate operation, a slow performance enhancement is seen until λ_{anode} of 1.6. Therefore, the

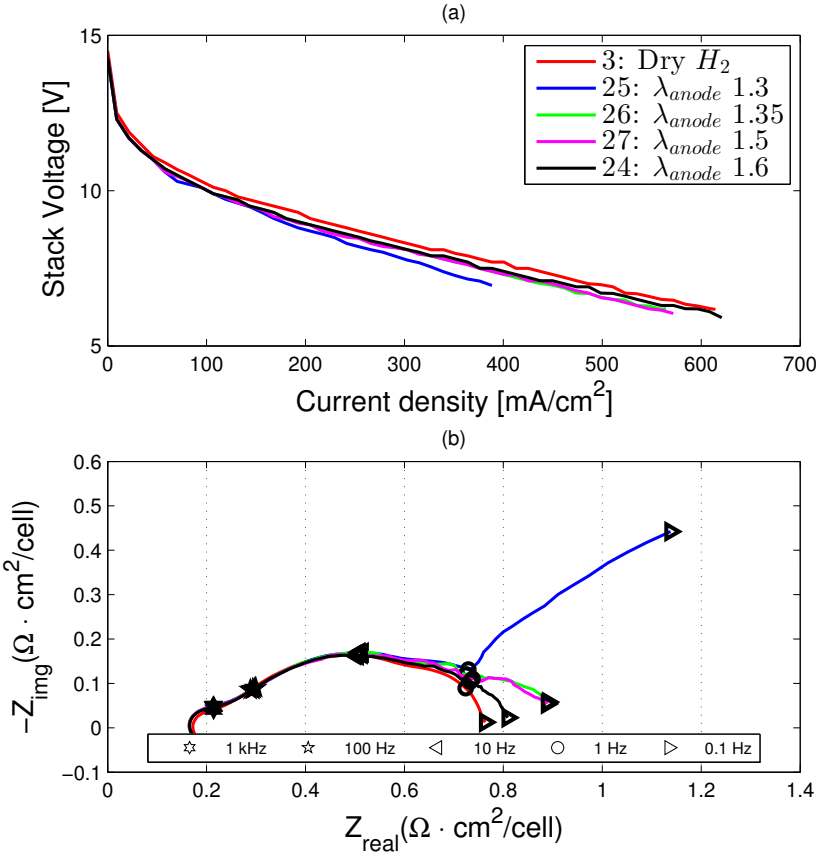

Figure 11. Impedance plot with different anode stochiometry levels with reformate gas

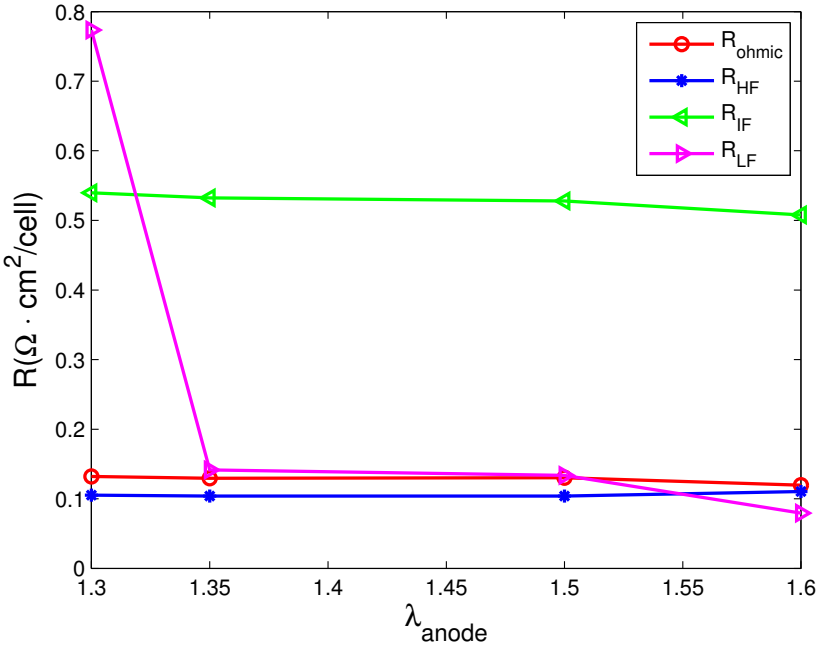

Figure 12. Effects of anode stoichiometry under reformate gas operation

proper operation under reformate condition should be done at higher stoichiometric ratio compared to dry hydrogen, in the current work around 1.6.

Cathode stoichiometry The effects of air stoichiometry on the fuel cell stack are similar to the ones seen for anode stoichiometry, mainly in the mass transport region. The polarization curves in Fig. 13(a) show a marked performance enhancement with increasing $\lambda_{cathode}$.

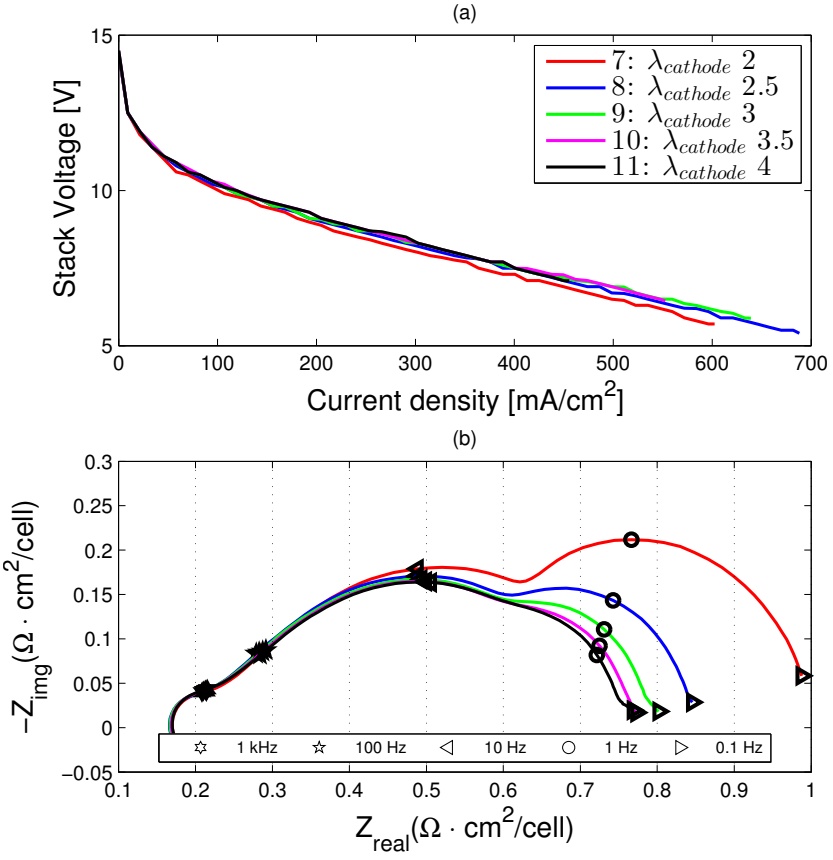

Figure 13. Impedance plot with different cathode stoichiometry levels with dry H2

The resistances in Fig. 14 show changes mostly in the low frequency region. As can be seen by the asymptotic trend in Fig. 14, R_{LF} decreases significantly when $\lambda_{cathode}$ increases from 2 to 3 and then slowly levels out until $\lambda_{cathode} = 4$. Unlike with λ_{anode}, changes in $\lambda_{cathode}$ provoke small changes in R_{ohmic} and R_{HF}, where small decrease of the former and increase of the latter are observed at $\lambda_{cathode} > 2.5$. However, both resistances return to similar values of $\lambda_{cathode} = 2$ when $\lambda_{cathode}$ increases to 4. These changes are not distinct or consistent enough to make conclusions on the effects of cathode stoichiometry on these resistances, but the effects are clearly captured on the low frequency region. As with anode stoichiometry, the effects decrease with increasing stoichiometric ratio, implying that once a sufficient mass transport is achieved, further increase in air stoichiometric ratio does not bring about performance enhancement. Similarly, Jespersen et al. [16] found that air stoichiometric ratios above four have little or no effect on the performance of a single cell.

Figure 15 shows the air stoichiometry test on reformate. The polarization curves show the difference between the different tests, where the increase in stoichiometric ratio improves the overall performance of the fuel cell stack. Likewise, the impedance spectra show a shrinking low frequency loops with increasing air stoichiometric ratio. This corresponds to decreasing R_{LF} in Fig. 16, where it decreases until $\lambda_{cathode}$

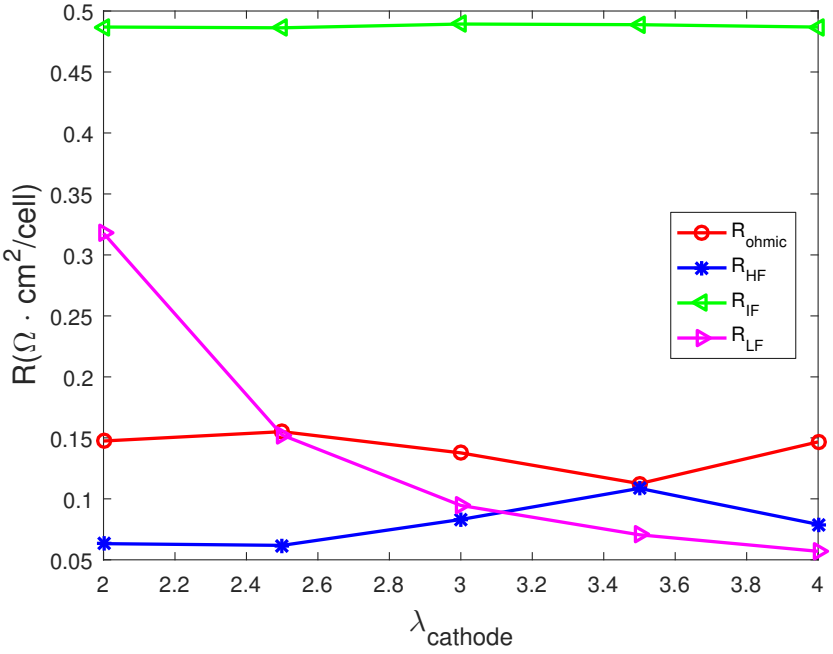

Figure 14. Effects of cathode stoichiometry under dry H_2 operation

= 3 and then levels out. This shows that even in the case of air stoichiometry once a sufficient mass transport is achieved further increase in stoichiometry does not produce significant performance increase. Jespersen et al. [16] made similar conclusions, where fuel cell performance enhances dramatically until $\lambda_{cathode} = 3$, and has little or no effects at $\lambda_{cathode} > 4$. Their tests were done on a unit cell assembly, however, the resistances are comparable as the stack impedances are normalized by the number of cells for comparability purposes in the current work.

The other resistances show small changes below $\lambda_{cathode} = 2.5$ and then remain unaltered for further increase in stoichiometric ratio. Since water vapor is present in the reformate gas, it is not clear whether these small changes at low stoichiometric ratios are due to the effects of stoichiometry on water transport [13]. However, the changes are too small for more detailed conclusions on the effects of stoichiometry on membrane and charge transfer resistances, except for the fact that they are not affected at $\lambda_{cathode} > 2.5$.

3.3 CO Poisoning

Results of reformate gas composition with varying CO content are presented in Fig. 17. CO concentration was varied between 0.25% and 1% by volume in the gas feed, and it can be seen from the polarization curves in Fig.17(a) and the Nyquist plot in Fig.17(b) that there is no significant CO poisoning effect. As can be expected the overall performance in the presence of CO is lower than dry H_2 provided other conditions are kept the same, Fig. 17. This is widely accepted to be due to surface adsorption of CO on Pt reaction sites [6, 17, 21].

In Fig. 18 the changes in the resistances are almost all negligible. There are slight changes in R_{LF}, which however, are too small to provide any insight towards the effects of CO on this frequency range, considering that at stack level and at low frequency measurement noises are more pronounced. At cell level, Andreasen et al. [2] found that CO affects negatively the entire impedance spectrum of an HT-PEMFC at the same frequency range as the present work. They attributed the causes to anode activation effects for high frequency region, and longer diffusion paths due to reduced Pt sites and consequently local variations in H_2 concentration in the catalyst for intermediate frequency, and lastly, the extension of these local variations in H_2 concentration to the gas channels for low frequency. However, in the present work most of the resistances remain unaltered, showing the robustness of HT-PEMFCs towards such concentrations of CO at stack level.

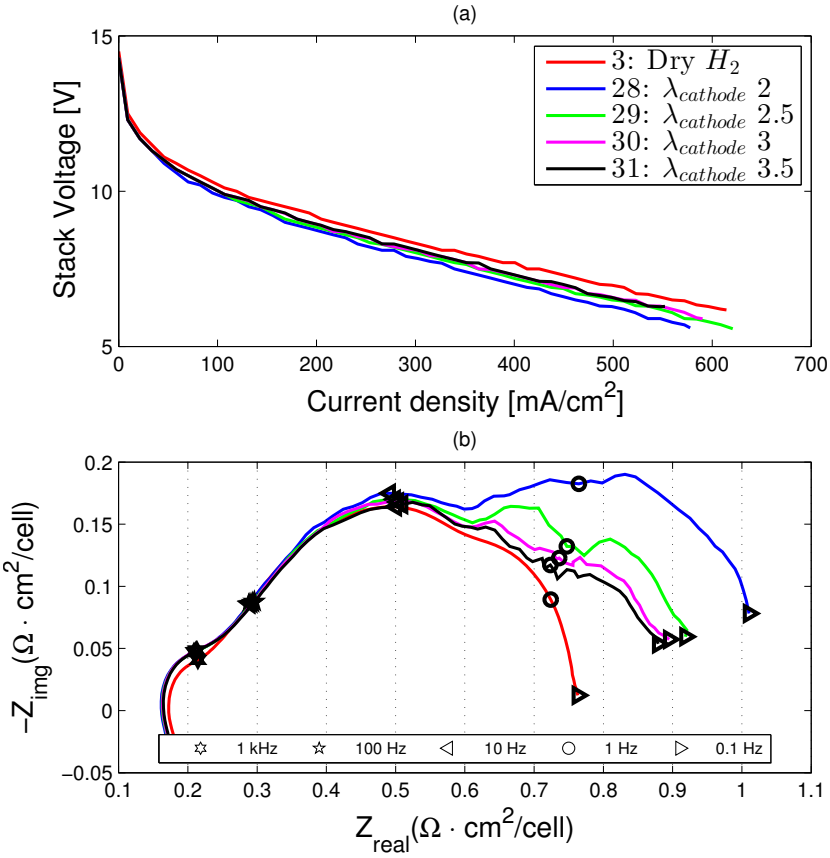

Figure 15. Impedance plot at different air stochiometry levels under SR gas operation

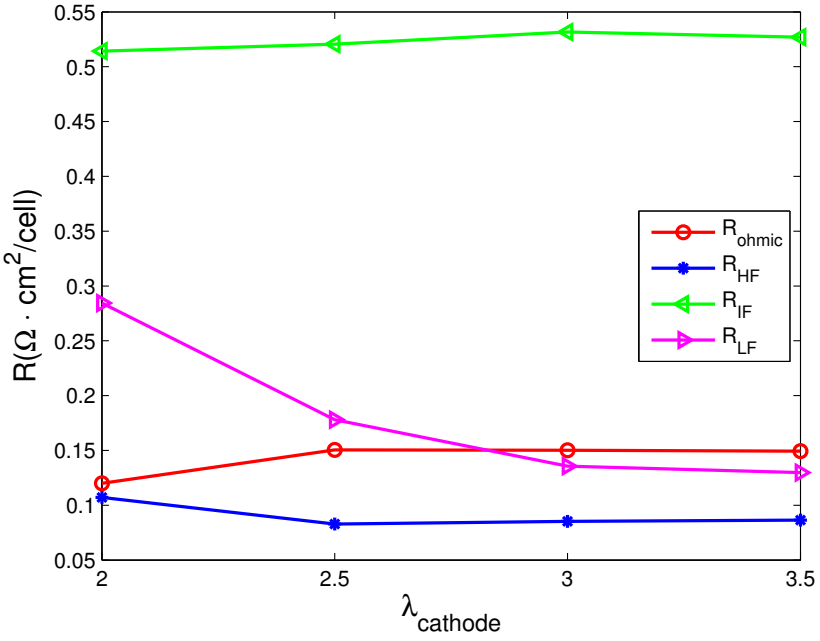

Figure 16. Effects of air stoichiometry under SR gas operation

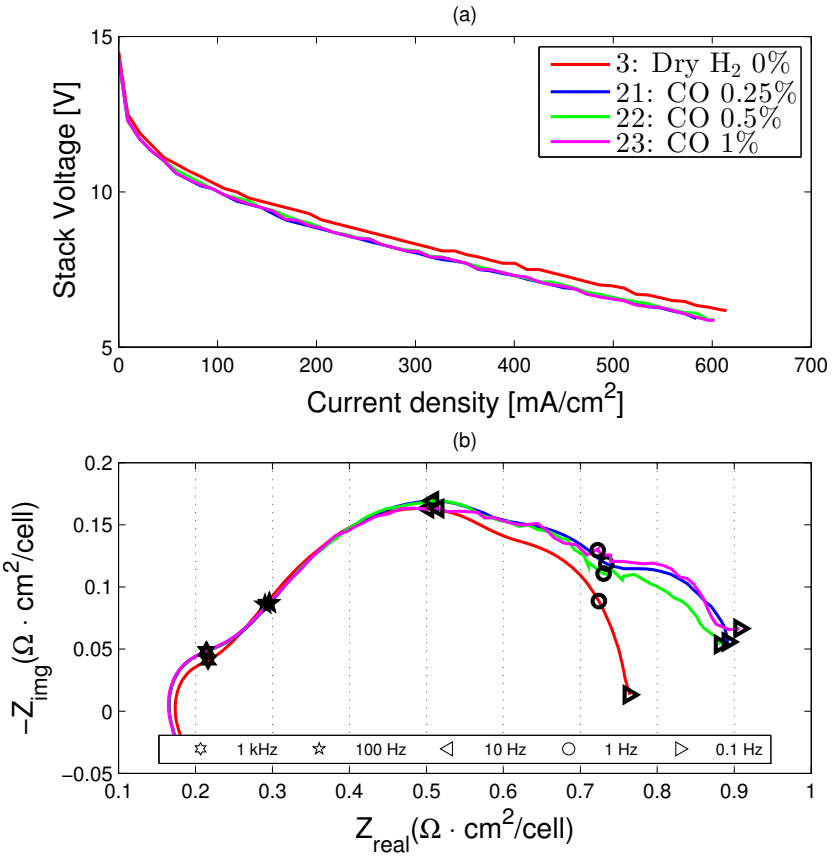

Figure 17. Polarization plot and impedance spectrum for varying CO content in reformate gas.

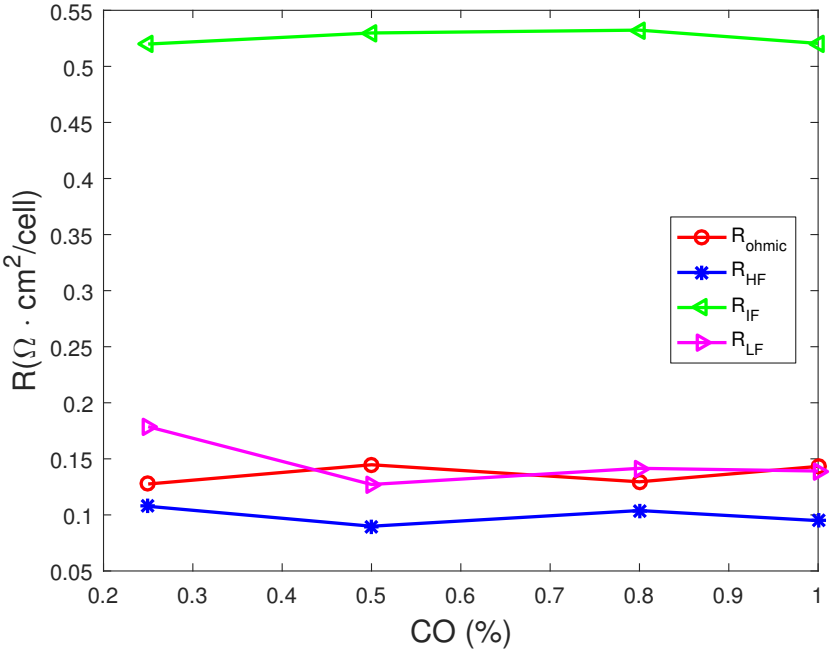

Figure 18. Effects of co concentration under reformate gas operation

3.4 Dry H_2, SR Gas and ATR Gas Operation Modes

Figures 19 and 20 show a comparison of different fuel compositions, namely; dry hydrogen, SR gas and ATR gas. It can be seen that the highest performance is obtained under dry H_2 operation and the poorest performance under ATR gas feed both for 160 °C and 170 °C. This can be explained by the reduced hydrogen content in the gas feed both in SR gas and ATR gas modes, 60% and 41%, respectively.

The most significant changes are seen below 10 Hz, showing that mass transport is the main issue. Changing between the different operation modes from dry H_2 to SR gas and then to ATR gas produces the same effects as decreasing λ_{anode} in Fig. 11. In fact, the two tests are similar. Since the effects of CO are small and similar between 0.25% and 1% as seen in Fig. 18, the amount of H_2 is the determinant factor in both tests. This also means that just as increasing λ_{anode} enhanced the performance during dry H_2 operation, it may improve the performance of both SR gas and ATR gas operation modes as well.

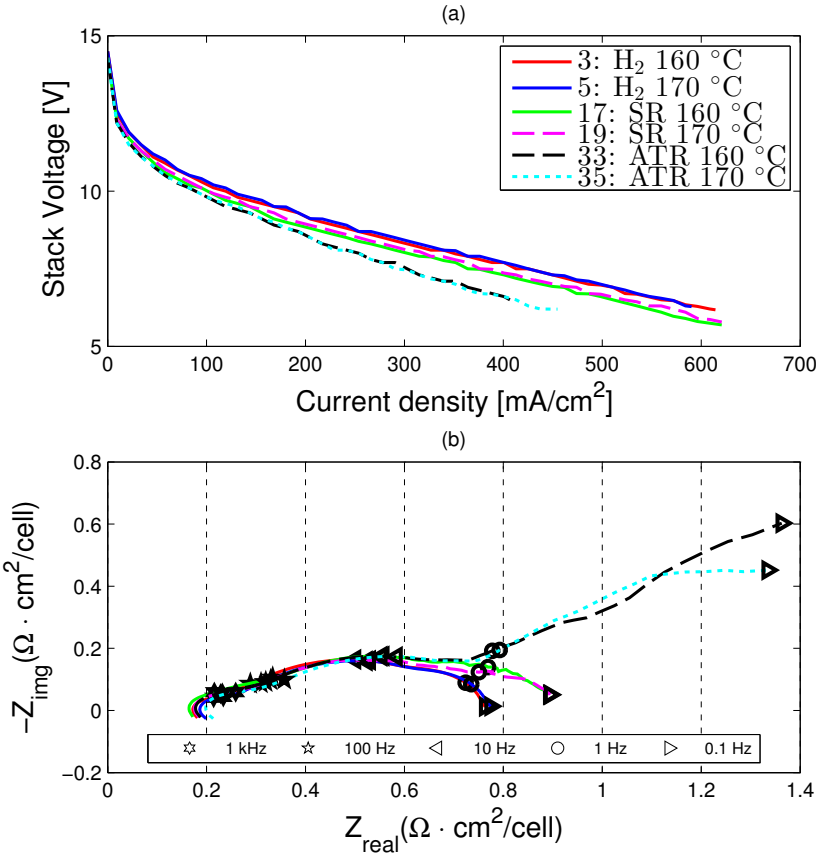

Figure 19. Impedance plots comparing for dry H_2, SR gas and ATR gas operation modes at 160 °C and 170 °C

4 Conclusion

This work investigates the effects of temperature, air stoichiometry and hydrogen stoichiometry under dry hydrogen and reformate gas operation modes on a PBI-based HT-PEMFC stack. Characterization was done by means of galvanostatic EIS and polariztion curves. An equivalent circuit was chosen based on the impedance response of the tested fuel cell stack for data analysis and interpretation.

Increase in temperature of relatively small 5 °C steps is seen to bring about only little enhancement in performance, both under dry H_2 and reformate gas operation modes. All the resistances remain almost

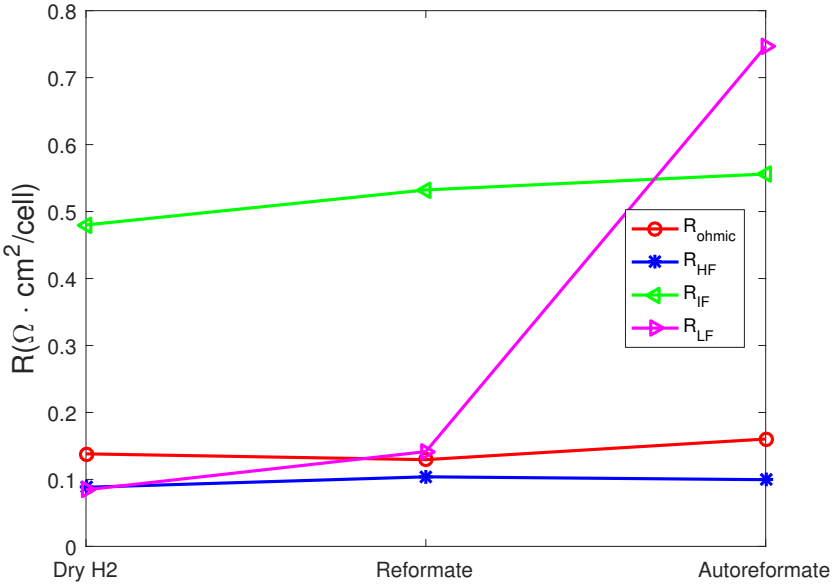

Figure 20. Comparison of dry H_2, SR gas and ATR gas operation modes at 160 $^{\circ}C$

unaltered with the exception of a slightly increasing ohmic resistance in both cases. It can be stated that the increase in ohmic resistance may affect the stack performance negatively, but the summation of the slight enhancements in the remaining frequency ranges compensate for it.

Stoichiometry on the other hand has a significant effect on the fuel cell stack performance. A hydrogen stoichiometry of 1.25 and 1.3, during dry H_2 and reformate gas operation modes, respectively show a 45° diffusion limitation line on the Nyquist plot. These are then easily corrected in both cases by an increase in hydrogen stoichiometry of 0.5. Mass transport limitation is also the main issue at lower air stoichiometries both under dry H_2 and reformate gas feeds. Even here increasing air stiochiometry enhances the performance significantly until the mass transport issues are minimized. It can be concluded that it is crucial that stoichiometric ratios are set to guarantee sufficient mass transport, but once that is achieved further increase of either anode or cathode stoichiometric ratio does not enhance the stack performance appreciably. In this work, sufficient mass transport is achieved at $\lambda_{anode} = 1.3$ for dry hydrogen, $\lambda_{anode} = 1.6$ for reformate operation and $\lambda_{cathode} = 4$.

CO poisoning was also studied. Even though, the performance in the presence of CO is slightly lower compared to dry H_2 operation, no poisoning effects were observed when increasing the CO content from 0.25% to 1% by volume in the reformate feed gas. Since the high frequency resistance that is expected to be most affected by anode poisoning remain unaltered it can be said that the stack is robust enough to concentrations of CO less than 1%.

When comparing different fuel compositions, namely, dry H_2, SR gas and ATR gas, they all performed in the expected order, with the first performing the best. Considering that the effects of CO poisoning are negligible until CO contents of 1% by volume, the mass transport limitation seen during SR gas and ATR gas operation modes are caused by the reduced H_2 content in the feed. The differences among the different operation modes are mass transport limited, similar to those seen when decreasing stoichiometries. Therefore, increasing anode stoichiometry may improve the performance of both SR gas and ATR gas operation modes. It is recommended to ensure sufficient mass transport in the fuel cell stack when operating under reformate conditions.

EIS can be an efficient tool for this purpose as one can compare impedance spectra of SR gas or ATR gas operation modes with dry H_2 impedance spectra and increase the anode stoichiometry until the mass transport behavior at low frequency matches that of a dry H_2 operation mode or ceases to improve the performance.

Acknowledgments The authors would like to thank the Danish Energy Technology Development and Demonstration Programme (EUDP) for funding this work through the Commercial Breakthrough of Advanced Fuel Cells Project (COBRA-2 (Grant number: 64012-0257)), and Serenergy A/S for supplying the fuel cell stack.

References

1. D. Aili, T. Allward, S. M. Alfaro, C. Hartmann-Thompson, T. Steenberg, H. A. Hjuler, Q. Li, J. O. Jensen, and E. J. Stark, "Polybenzimidazole and sulfonated polyhedral oligosilsesquioxane composite membranes for high temperature polymer electrolyte membrane fuel cells," *Electrochimica Acta*, vol. 140, pp. 182–190, 2014. [Online]. Available: http://dx.doi.org/10.1016/j.electacta.2014.03.047
2. S. J. Andreasen, J. R. Vang, and S. K. Kær, "High temperature PEM fuel cell performance characterisation with CO and CO2 using electrochemical impedance spectroscopy," *International Journal of Hydrogen Energy*, vol. 36, no. 16, pp. 9815–9830, aug 2011. [Online]. Available: http://www.sciencedirect.com/science/article/pii/S0360319911009414
3. S. S. Araya, S. J. Andreasen, and S. K. Kær, "Experimental characterization of the poisoning effects of methanol-based reformate impurities on a PBI-based high temperature PEM fuel cell," *Energies*, vol. 5, no. 12, pp. 4251–4267, Oct. 2012. [Online]. Available: http://www.mdpi.com/1996-1073/5/11/4251/http://www.mdpi.com/1996-1073/5/11/4251/pdfhttp://www.scopus.com/inward/record.url?eid=2-s2.0-84868606449&partnerID=tZOtx3y1
4. S. Authayanun, K. Im-orb, and A. Arpornwichanop, "A review of the development of high temperature proton exchange membrane fuel cells," *Chinese Journal of Catalysis*, vol. 36, no. 4, pp. 473–483, Apr. 2015. [Online]. Available: http://linkinghub.elsevier.com/retrieve/pii/S1872206714602722
5. M. Boaventura and A. Mendes, "Activation procedures characterization of MEA based on phosphoric acid doped PBI membranes," *International Journal of Hydrogen Energy*, vol. 35, no. 20, pp. 11 649–11 660, Oct. 2010. [Online]. Available: http://linkinghub.elsevier.com/retrieve/pii/S0360319910006555
6. S. Bose, T. Kuila, T. X. H. Nguyen, N. H. Kim, K.-t. Lau, and J. H. Lee, "Polymer membranes for high temperature proton exchange membrane fuel cell: Recent advances and challenges," *Progress in Polymer Science*, vol. 36, no. 6, pp. 813–843, Jun. 2011. [Online]. Available: http://linkinghub.elsevier.com/retrieve/pii/S0079670011000256
7. A. Chandan, M. Hattenberger, A. El-kharouf, S. Du, A. Dhir, V. Self, B. G. Pollet, A. Ingram, and W. Bujalski, "High temperature (HT) polymer electrolyte membrane fuel cells (PEMFC) âĂŞ A review," *Journal of Power Sources*, vol. 231, pp. 264–278, Jun. 2013. [Online]. Available: http://linkinghub.elsevier.com/retrieve/pii/S0378775312018113
8. M. K. Daletou, J. K. Kallitsis, G. Voyiatzis, and S. G. Neophytides, "The Interaction of Water Vapors with H3PO4 Imbibed Electrolyte Based on PBI/polysulfone Copolymer Blends," *Journal of Membrane Science*, vol. 326, no. 1, pp. 76–83, 2009.
9. M. K. Daletou, J. Kallitsis, and S. G. Neophytides, *Interfacial Phenomena in Electrocatalysis*, ser. Modern Aspects of Electrochemistry, C. G. Vayenas, Ed. New York, NY: Springer New York, 2011, vol. 51. [Online]. Available: http://link.springer.com/10.1007/978-1-4419-5580-7
10. J.-L. Dellis, "z-Fit for Matlab." [Online]. Available: https://se.mathworks.com/matlabcentral/fileexchange/19460-zfit
11. B. Du, R. Pollard, J. F. Elter, and M. Ramani, "Performance and Durability of a Polymer Electrolyte Fuel Cell Operating with Reformate: Effects of CO, CO2, and Other Trace Impurities," *Polymer Electrolyte Fuel Cell Durability*, pp. 341–366, 2009. [Online]. Available: http://dx.doi.org/10.1007/978-0-387-85536-3_17
12. Y. Ferng, A. Su, and J. Hou, "Parametric investigation to enhance the performance of a PBI-based high-temperature PEMFC," *Energy Conversion and Management*, vol. 78, pp. 431–437, Feb. 2014. [Online]. Available: http://www.sciencedirect.com/science/article/pii/S0196890413007048
13. S. Galbiati, A. Baricci, A. Casalegno, G. Carcassola, and R. Marchesi, "On the activation of polybenzimidazole-based membrane electrode assemblies doped with phosphoric acid," *International Journal of Hydrogen Energy*, vol. 37, no. 19, pp. 14 475–14 481, Oct. 2012. [Online]. Available: http://linkinghub.elsevier.com/retrieve/pii/S0360319912016096
14. J. Hu, H. Zhang, Y. Zhai, G. Liu, and B. Yi, "500h Continuous aging life test on PBI/H3PO4 high-temperature PEMFC," *International Journal of Hydrogen Energy*, vol. 31, no. 13, pp. 1855–1862, Oct. 2006.
15. T. Iwasita, "Methanol and CO electrooxidation," in *Handbook of Fuel Cells - Fundamentals, Technology, and Applications*, 2003, vol. 2, pp. 603–624.
16. J. L. Jespersen, E. Schaltz, and S. K. Kær, "Electrochemical characterization of a polybenzimidazole-based high temperature proton exchange membrane unit cell," *Journal of Power Sources*, vol. 191, no. 2, pp. 289–296, jun 2009. [Online]. Available: http://www.sciencedirect.com/science/article/pii/S0378775309002742

17. S. Kaserer, C. Rakousky, J. Melke, and C. Roth, "Design of a reference electrode for high-temperature PEM fuel cells," *Journal of Applied Electrochemistry*, vol. 43, no. 11, pp. 1069–1078, May 2013. [Online]. Available: http://link.springer.com/10.1007/s10800-013-0567-9
18. M. S. Kondratenko, M. O. Gallyamov, and A. R. Khokhlov, "Performance of high temperature fuel cells with different types of PBI membranes as analysed by impedance spectroscopy," *International Journal of Hydrogen Energy*, vol. 37, no. 3, pp. 2596–2602, 2012. [Online]. Available: http://dx.doi.org/10.1016/j.ijhydene.2011.10.087
19. A. R. Korsgaard, M. P. Nielsen, M. Bang, and S. K. Kær, "Modeling of CO influence in PBI electrolyte PEM fuel cells," in *Proceedings of the 4th International ASME Conference on Fuel Cell Science, Engineering and Technology*. ASME Press, 2006.
20. J.-h. Lee, J.-H. Lee, W. Choi, K.-W. Park, H.-Y. Sun, and J.-H. Oh, "Development of a method to estimate the lifespan of proton exchange membrane fuel cell using electrochemical impedance spectroscopy," *Journal of Power Sources*, vol. 195, no. 18, pp. 6001–6007, Sep. 2010. [Online]. Available: http://linkinghub.elsevier.com/retrieve/pii/S0378775310003137
21. Q. Li, R. He, J.-A. Gao, J. O. Jensen, and N. J. Bjerrum, "The CO Poisoning Effect in PEMFCs Operational at Temperatures up to 200ÂřC," *Journal of The Electrochemical Society*, vol. 150, no. 12, p. A1599, Dec. 2003. [Online]. Available: http://jes.ecsdl.org/content/150/12/A1599.full
22. Q. Li, J. O. Jensen, R. F. Savinell, and N. J. Bjerrum, "High Temperature Proton Exchange Membranes Based on Polybenzimidazoles for Fuel Cells," *Progress in Polymer Science*, vol. 34, no. 5, pp. 449 – 477, 2009.
23. H. Liu, P. Li, A. Hartz, and K. Wang, "Effects of geometry/dimensions of gas flow channels and operating conditions on high-temperature PEM fuel cells," *International Journal of Energy and Environmental Engineering*, Nov. 2014. [Online]. Available: http://link.springer.com/10.1007/s40095-014-0153-x
24. V. P. McConnell, "High-temperature PEM fuel cells: Hotter, simpler, cheaper," *Fuel Cells Bulletin*, vol. 2009, no. 12, pp. 12–16, Dec. 2009. [Online]. Available: http://linkinghub.elsevier.com/retrieve/pii/S1464285909704110
25. M. M. Mench, E. C. Kumbur, T. N. Veziroglu, and S. S. Kocha, *Polymer Electrolyte Fuel Cell Degradation*. Elsevier, 2012. [Online]. Available: http://www.sciencedirect.com/science/article/pii/B978012386936410003X
26. B. Najafi, A. Haghighat Mamaghani, A. Baricci, F. Rinaldi, and A. Casalegno, "Mathematical modelling and parametric study on a 30ÂăkWel high temperature PEM fuel cell based residential micro cogeneration plant," *International Journal of Hydrogen Energy*, vol. 40, no. 3, pp. 1569–1583, Jan. 2015. [Online]. Available: http://www.sciencedirect.com/science/article/pii/S0360319914032273
27. M. Orazem and B. Tribollet, *Electrochemical impedance spectroscopy*. Wiley-Interscience, 2008, vol. 48. [Online]. Available: http://books.google.com/books?hl=en&lr=&id=AEwQuNTZZ-MC&oi=fnd&pg=PR15&dq=Electrochemical+Impedance+Spectroscopy&ots=BObQhI_2NH&sig=FOgZf4Y-r9UfcRHsuxVXf9pg6Sc
28. A. Orfanidi, M. K. Daletou, L. Sygellou, and S. G. Neophytides, "The role of phosphoric acid in the anodic electrocatalytic layer in high temperature PEM fuel cells," *Journal of Applied Electrochemistry*, vol. 43, no. 11, pp. 1101–1116, Oct. 2013. [Online]. Available: http://link.springer.com/10.1007/s10800-013-0626-2
29. M. Pérez-Page and V. Pérez-Herranz, "Study of the electrochemical behaviour of a 300 W PEM fuel cell stack by Electrochemical Impedance Spectroscopy," *International Journal of Hydrogen Energy*, 2014. [Online]. Available: http://www.sciencedirect.com/science/article/pii/S0360319913013530
30. T. Romero-Castañón, L. Arriaga, and U. Cano-Castillo, "Impedance spectroscopy as a tool in the evaluation of MEAs," *Journal of Power Sources*, vol. 118, no. 1-2, pp. 179–182, May 2003. [Online]. Available: http://www.sciencedirect.com/science/article/pii/S0378775303000855
31. L. Salemme, L. Menna, and M. Simeone, "Calculation of the energy efficiency of fuel processor: PEM (proton exchange membrane) fuel cell systems from fuel elementar composition and heating value," *Energy*, vol. 57, pp. 368–374, aug 2013. [Online]. Available: http://www.sciencedirect.com/science/article/pii/S0360544213003332
32. Serenergy A/S, "Datasheet S165L Liquid cooled HTPEM stack," pp. 1–2, 2014. [Online]. Available: http://serenergy.com/
33. Y. Shao, G. Yin, Z. Wang, and Y. Gao, "Proton exchange membrane fuel cell from low temperature to high temperature: Material challenges," *Journal of Power Sources*, vol. 167, no. 2, pp. 235–242, May 2007. [Online]. Available: http://www.sciencedirect.com/science/article/pii/S0378775307004715
34. C. Siegel, I. Buder, and A. Heinzel, "Sectional electrochemical impedance analysis of a high temperature polymer electrolyte membrane fuel cell with three types of flow-fields," *Electrochimica Acta*, 2013. [Online]. Available: http://www.sciencedirect.com/science/article/pii/S0013468613016721
35. S. Simon Araya, S. Juhl Andreasen, H. Venstrup Nielsen, and S. Knudsen Kær, "Investigating the effects of methanol-water vapor mixture on a PBI-based high temperature PEM fuel cell," *Int. J. Hydrogen Energy*, vol. 37, no. 23, pp. 18 231–18 242, Dec. 2012. [Online]. Available: http://linkinghub.elsevier.com/retrieve/pii/S0360319912020125

36. S. Simon Araya, I. F. Grigoras, F. Zhou, S. J. Andreasen, and S. K. Kær, "Performance and endurance of a high temperature PEM fuel cell operated on methanol reformate," *International Journal of Hydrogen Energy*, pp. 2–9, 2014.
37. C. Song, S. R. Hui, and J. Zhang, "High-temperature PEM Fuel Cell Catalysts and Catalyst Layers," in *PEM Fuel Cell Electrocatalysts and Catalyst Layers: Fundamentals and Applications*. Springer London, 2008, pp. 861–888.
38. A. Su, Y. M. Ferng, J. Hou, and T. L. Yu, "Experimental and numerical investigations of the effects of PBI loading and operating temperature on a high-temperature PEMFC," *International Journal of Hydrogen Energy*, vol. 37, no. 9, pp. 7710–7718, May 2012. [Online]. Available: http://www.sciencedirect.com/science/article/pii/S0360319912003011
39. J. R. Vang, S. J. Andreasen, S. Simon Araya, and S. K. Kær, "Comparative study of the break in process of post doped and solâĂŞgel high temperature proton exchange membrane fuel cells," *International Journal of Hydrogen Energy*, vol. 39, no. 27, pp. 14 959–14 968, Aug. 2014. [Online]. Available: http://www.sciencedirect.com/science/article/pii/S0360319914019727
40. X.-Z. Yuan, C. Song, H. Wang, and J. Zhang, *Electrochemical Impedance Spectroscopy in PEM Fuel Cells*. London: Springer London, 2010. [Online]. Available: http://www.springerlink.com/index/10.1007/978-1-84882-846-9
41. X. Yuan, H. Wang, J. C. Sun, and J. Zhang, "AC impedance technique in PEM fuel cell diagnosis–A review," *International Journal of Hydrogen Energy*, vol. 32, no. 17, pp. 4365–4380, 2007. [Online]. Available: http://www.sciencedirect.com/science/article/B6V3F-4P5YK26-1/2/8d98edc8e2b445980931039f7cb4c716
42. C. Zhang, Z. Liu, W. Zhou, S. H. Chan, and Y. Wang, "Dynamic performance of a high-temperature PEM fuel cell - An experimental study," *Energy*, vol. 90, pp. 1949–1955, 2015.
43. J. Zhang, Z. Xie, J. Zhang, Y. Tang, C. Song, T. Navessin, Z. Shi, D. Song, H. Wang, D. P. Wilkinson, Z. S. Liu, and S. Holdcroft, "High temperature PEM fuel cells," *Journal of Power Sources*, vol. 160, no. 2 SPEC. ISS., pp. 872–891, 2006.
44. J. Zhang, T. Thampan, and R. Datta, "Influence of Anode Flow Rate and Cathode Oxygen Pressure on CO Poisoning of Proton Exchange Membrane Fuel Cells," *Journal of The Electrochemical Society*, vol. 149, no. 6, p. A765, 2002.
45. Y. Zhu, W. Zhu, and B. Tatarchuk, "Performance comparison between high temperature and traditional proton exchange membrane fuel cell stacks using electrochemical impedance spectroscopy," *Journal of Power Sources*, 2014. [Online]. Available: http://www.sciencedirect.com/science/article/pii/S037877531400072X

